Emergent Materials (2024) 7:937–946
https://doi.org/10.1007/s42247-024-00654-9

ORIGINAL ARTICLE

Visible light-induced H_2 production and pollutant degradation by copper oxide nanosphere embedded zinc-cadmium-sulfide composite

Muhammad Imran[1,2] · Ammar Bin Yousaf[3] · Muhammad Farooq[4] · Samaira Kausar[5] · Samina Yasmeen[5] · Peter Kasak[3]

Received: 10 October 2023 / Accepted: 13 February 2024 / Published online: 11 March 2024

Abstract

Green hydrogen production using solar water splitting and solving water pollution issues are intricately intertwined global goals which are hindered by the scarcity of highly active photocatalytic materials. Herein, we have presented a simple strategy to couple two semiconductors (Cu_2O and ZnCdS) to form a type-I heterojunction with high visible light response. The as-synthesized heterojunction was well characterized by the battery techniques, such as TEM, HAADF-STEM elemental mapping, XRD and XPS. The visible light response was higher for composite than individual components, as was also supported by UV–vis DRS. The Cu_2O-ZnCdS composite showed a higher visible light-driven photocatalytic H_2 production rate (78.5 μmol g^{-1} h^{-1}). The catalyst was also active for photocatalytic degradation of a model dye-methylene blue (MB)-with a degradation rate constant of 0.079 min^{-1}. The enhanced performance of the Cu_2O-loaded ZnCdS catalysts can be ascribed to both factors, such as enhancement of the visible light absorption and the growth of Cu_2O-ZnCdS heterojunction. The heterojunction formation facilitates efficient charge separation with smaller charge resistance, as evidenced by transient photocurrent response and electrochemical impedance spectroscopy (EIS) studies. This study strongly indicates that the photocatalytic reactions with this catalyst material are kinetically favoured by coupling the two semiconductors.

Keywords Heterojunction · H_2 production · Dye degradation · Photocatalysis · Semiconductors

1 Introduction

Climate change and water pollution are inextricably linked entities, and the current situation of our Earth needs the utilization of both renewable energy and the formation of novel materials for water purification [1, 2]. Hydrogen (H_2) has been recognized as one of the most reliable clean energy carriers that can replace fossil fuels. Hydrogen energy has found extensive applications in various industries such as petroleum, chemical, energy, and transportation. However, carbon dioxide and other greenhouse gases are released during the steam reforming process for hydrogen production [3, 4]. Over the last few decades, green hydrogen (hydrogen generated without greenhouse gases emission) production techniques, such as water thermolysis, photolysis, and electrolysis, have gained a lot of interest from the scientific community [5–9]. Among all green techniques, photocatalytic water splitting is a promising technology due to its more straightforward, cheaper, and scalable system design and operation [10].

Muhammad Imran and Ammar Bin Yousaf contributed equally to this work.

✉ Muhammad Farooq
mufaroouk@gmail.com; 20hs109g@shinshu-u.ac.jp

✉ Peter Kasak
peter.kasak@qu.edu.qa

1 Hefei National Laboratory for Physical Sciences at Microscale, University of Science and Technology of China, Hefei, Anhui 230026, People's Republic of China

2 Clean Energy Research Center, University of Yamanashi, Kofu 400-8510, Japan

3 Center for Advanced Materials, Qatar University, 2713 Doha, Qatar

4 Interdisciplinary Graduate School of Science and Technology, Shinshu University, Ueda 386-8567, Japan

5 Department of Chemistry, National Science College, Satellite Town, Gujranwala 52250, Pakistan

Moreover, water contamination by industrial waste significantly harms aquatic life systems and human health. The most frequent effluent that the textile and printing industries discharge into water bodies is dye, which has a bright hue, complex aromatic structure and resistance to light, heat and chemicals [11–13]. Therefore, removing those dangerous dyes from water is crucial. There are several traditional ways of degrading these effluents. Still, they are less efficient due to their high maintenance and operational costs and high concentration of phenolic and aromatic rings in dye molecules, making them harder to degrade [14, 15]. Compared to these conventional approaches, the photocatalytic oxidation process might be considered a good alternative with great efficiency and simpler design [16].

It would be interesting to see a photocatalyst that could act both for photocatalytic H_2 production and dye degradation for water purification. One such promising visible light active semiconductor is Cu_2O, which has received widespread recognition for its use in various fields, including photocatalysis, photo-electrocatalysis and water splitting [17–19]. Due to its small bandgap (2.0–2.4 eV), Cu_2O has a significant potential for capturing solar energy. The energy efficiency is further improved by forming heterojunction band alignment of Cu_2O with other semiconductors [20, 21]. These characteristics are necessary to effectively enhance photogenerated electron–hole pair separation, leading to enhanced degradation efficiency. Until now, several semiconductors, including metal oxides, metal sulfides, metal nitrides, and carbon nitride, TiO_2-based photocatalysts have been well-researched [22, 23]. However, metal sulfide stands out among them for oxide combination photocatalysts due to its exceptional photocatalytic capability [24–26]. ZnCdS could be one example of a promising photocatalyst for heterojunction formation due to its adequate bandgap, appropriate band edge position, and strong visible light response. However, it is often difficult to get pure Cu_2O in the heterostructure using a facile strategy, given the three oxidation states of Cu species that are often displayed in a composite. Moreover, the complex fabrication process usually raises the overall cost of the system [27, 28].

Herein, we have presented a simple strategy to synthesize the Cu_2O nanosphere and loaded ZnCdS nanoparticles to form a heterojunction composite. The heterostructure composite (Cu_2O-ZnCdS) was used for photocatalytic H_2 production and methylene blue (MB) dye degradation.

2 Experimental

Detailed materials characterization information and application details have been provided in the supporting information file.

2.1 Preparation of Cu_2O nanosphere

The Cu_2O nanospheres were synthesized as follows: first, 0.01 mol of copper(II) acetate monohydrate and 1 g PVP (K-15) were mixed into 50 mL diethylene glycol. After a clean solution formation, then the mixture was heated up to 175 °C under N_2 atmosphere and maintained at that constant temperature for 2 h. Afterwards, the mixture was cooled down to room temperature, the precipitate was collected with centrifugation, washed with ethanol, and dried in a vaccum oven.

2.2 Preparation of Cu_2O-ZnCdS heterostructure

The heterostructured Cu_2O and ZnCdS was synthesized by using our previous protocol [29] described briefly as follows. Firstly, the Cu_2O nanosphere were dispersed in DI water, afterwards, the Zn, Cd and sulfide precursors were added dropwise simultaneously to get the 10wt% of ZnCdS. After completion of the addition, the samples were centrifugated and washed (with water and ethanol) and dried in a vacuum oven.

3 Results and discussion

The size and morphologies of Cu_2O-ZnCdS heterostructure in the as-synthesized samples [27] were investigated first by transmission electron microscopy (TEM) and scanning electron microscope (SEM). Figure S1 shows the SEM and TEM images of the Cu_2O nanospheres, which are about 200–300 nm in size and have spherical morphology. Figure S1c shows the SEM image of ZnCdS, which is about 10–20 nm in size and has an irregular shape. (Figure S1c) As can be seen in Fig. 1a and Figure S1d, the Cu_2O-ZnCdS composite exhibited spherical morphology with ZnCdS nanoparticles surrounding the Cu_2O nanosphere. The high-resolution image shows the Cu_2O nanospheres and ZnCdS are made up of prismatic bulge-like structures in closely packed arrays. (Fig. 1b) However, it was difficult to distinguish between ZnCdS and Cu_2O, which might lead to them being packed together. Therefore, the HAADF-STEM element mapping technique was employed to confirm the homogeneous and stable dispersion of ZnCdS onto the Cu_2O nanosphere. The elemental distribution for individual elements scan for the selected area has been taken in element mapping images for all the metals enclosed in the catalyst material presented in Fig. 1c-g. The overlay image derived from element mapping images presented in Fig. 1h showed that the ZnCdS is homogenously distributed onto the Cu_2O nanosphere. The characteristics of homogeneity in the

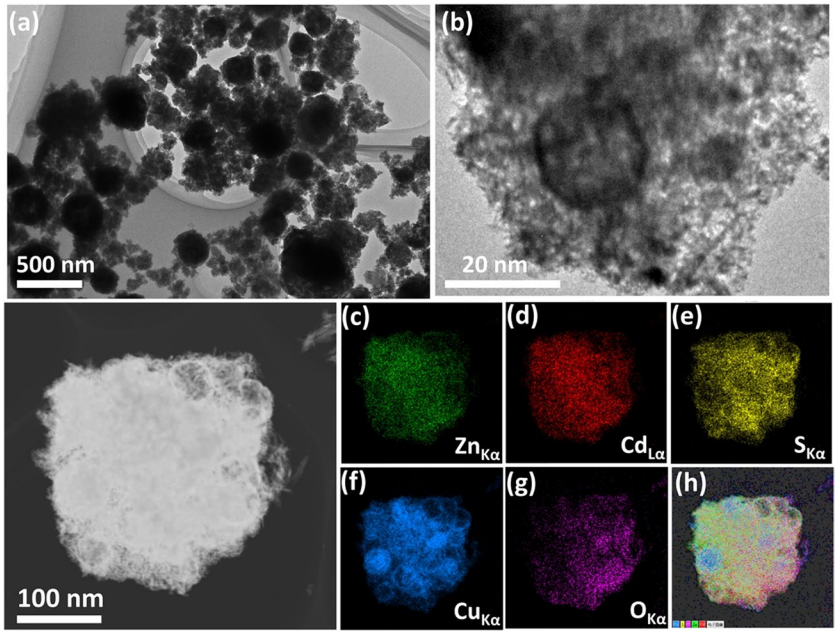

Fig. 1 TEM image for as-prepared Cu_2O-ZnCdS sample at lower (**a**) and higher magnifications (**b**), SAEED area element mapping images for individual elements i-e Zn, Cd, S, Cu & O, respectively (**c-g**), overlay image for element mapping (**h**)

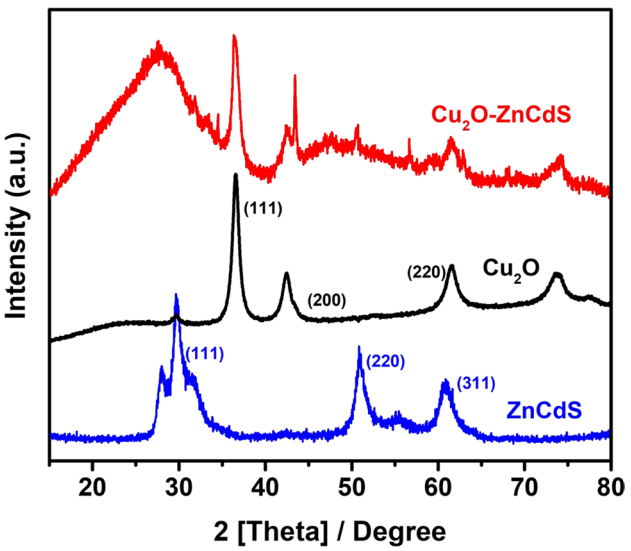

Fig. 2 XRD spectrum for Cu_2O nanosphere, ZnCdS nanoparticles and Cu_2O-ZnCdS samples

morphology results may correlate with possible metal-to-metal interactions and the support material for the successful mutual transference of electrons and better ductile behavior required for photocatalytic reaction.

Further, the powder X-ray diffraction analysis (XRD) of as-prepared samples was done to confirm the crystal structure. The XRD results of Cu_2O, ZnCdS and Cu_2O-ZnCdS samples are given in Fig. 2. The XRD data of the Cu_2O nanosphere is in good agreement with the literature (Cu_2O: JCPDS NO. 65–3288) with five typical peaks proportions located at 29.6°, 36.5°, 42.4°, 61.4° and 73.6° attributed to (110), (111), (200), (220) and (311) planes ascribed to Cu_2O, respectively [30, 31]. No clear features of Cu or CuO could be observed in the XRD spectrum, indicating that the products obtained consist of only the Cu_2O phase. The XRD spectrum of the Cu_2O-ZnCdS sample is also well matched with the cubic Zinc blend phase (ICSD # 80–0020) where peaks indexed at 27.34°, 45.32° and 53.66° correspond to (111), (220) and (311) planes, respectively [32]. The XRD of Cu_2O-ZnCdS shows diffraction peaks of both ZnCdS and Cu_2O phases, indicating a composite formation. However, additional diffraction peaks appearing at $2\theta = 43.3°$ and 50.5° correspond to the (111) and (200) plane of Cu (Cu: JCPDS NO. 04–0836), indicating the presence of the impurity phase [33].

Further, XPS analysis was also carried out to evaluate the chemical composition of the elements in the composite catalyst material's surfaces, their valance states, and the possible interactions influencing the photocatalytic performance. Figure S2 shows the survey scans for the Cu_2O-ZnCdS sample, presenting the existence of Cu, O, Zn, Cd and S in agreement with our findings from HAADF-STEM elemental mapping. Figure 3a shows the core-level spectra of Cu2p showing the typical characteristic peaks for Cu_2O at 932.54 and 952.71 eV, ascribed to $Cu2p_{3/2}$ and $Cu2p_{1/2}$, respectively. The broad peak raised at a higher binding energy side was also observed and characterized as a satellite peak and correlated to the presence of CuO and a minuscule amount of $Cu(OH)_2$ considered as the possible surface interaction between atmospheric oxygen and water vapour [34, 35]. The high-resolution XPS spectrum of O1s also shows a peak centered at 530.07 eV, assigned to lattice oxygen of Cu–O bonds (Fig. 3b), while the higher

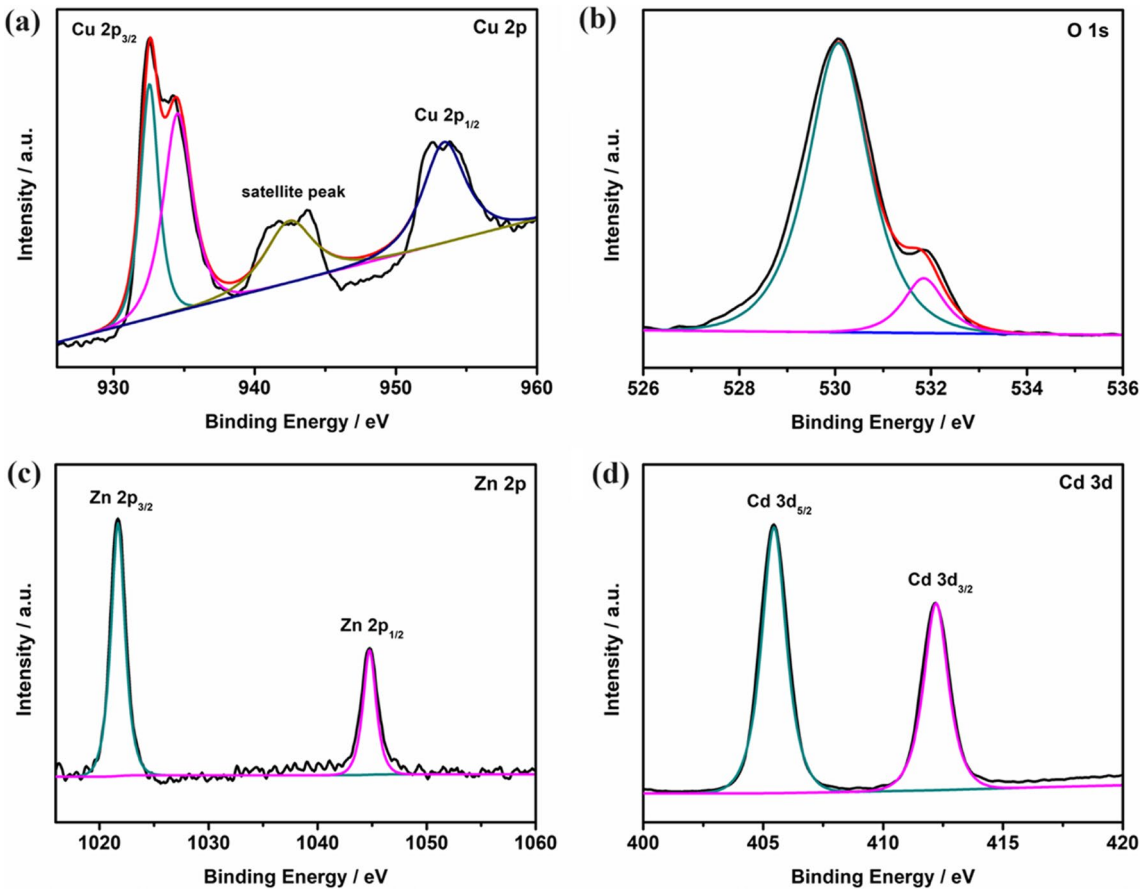

Fig. 3 XPS high-resolution scans for Cu_2O-ZnCdS sample at Cu2p (**a**), O1s (**b**), Zn2p (**c**) and Cd3d (**d**) region

binding energy region could be considered oxygen (from surface adsorbed O_2) that is coupled with water and CO_2 in the form of O–H and O–C groups, respectively [36, 37]. The high-resolution XPS spectrum of Zn2p shows peaks centered at 1021.70 eV & 1044.77 eV, typical for $2p_{3/2}$ and $2p_{1/2}$ components, respectively. The Cd3d spectrum also contains $3d_{5/2}$ & $3d_{3/2}$ spin–orbit components at 405.45 eV & 412.21 eV, respectively [38]. (Fig. 3c,d) The obtained XPS results are in good agreement with the XRD analysis and confirm composite formation. The amount of ZnCdS was also confirmed by XPS and ICP analysis, which shows a value of 7.8wt% and 9.1wt%, respectively, close to the experimentally adjusted value of 10wt%.

Having confirmed the composite's morphology, crystal structure and elemental composition, UV–vis DRS analysis were also performed to obtain the optical properties and understand the electronic transition and visible light response [39]. The UV–vis DRS spectra for pristine Cu_2O, ZnCdS and Cu_2O-ZnCdS composite are shown in Fig. 4. The Cu_2O shows strong absorption in the visible region (peak around 460 nm) with a green colour (Fig. 4a, inset a), while the ZnCdS sample exhibits lower visible absorption efficiency (yellow colour, Fig. 4a, inset b). However, after composite formation, the Cu_2O-ZnCdS showed intense brown colour (Fig. 4a inset c) and the absorption edge moved towards a higher wavelength (Fig. 4a). The corresponding band gap values were also calculated, and Cu_2O and ZnCdS showed a value of 2.0 eV and 2.25 eV, respectively (Fig. 4b). From UV–vis DRS, it is evident that the Cu_2O-ZnCdS composite showed lower band gap value and higher visible light absorbance, leading to a significant enhancement in the photocatalytic response.

The photocatalytic activity for H_2 production of Cu_2O, ZnCdS and Cu_2O-ZnCdS was investigated under the irradiations of visible light. Figure 5a exhibits the generation of hydrogen that is time-dependent, the amount of produced H_2 increased linearly with irradiation time for all the samples. The Cu_2O and ZnCdS showed photocatalytic hydrogen production rates of 34.7 μmol g^{-1} h^{-1} and 12.3 μmol g^{-1} h^{-1}, respectively. The photocatalytic H_2 production rate of the Cu_2O-ZnCdS sample was determined to be 78.5 μmol g^{-1} h^{-1}, which was about two times higher than pristine Cu_2O and six times higher than ZnCdS. This shows that combining individual photocatalysts to form

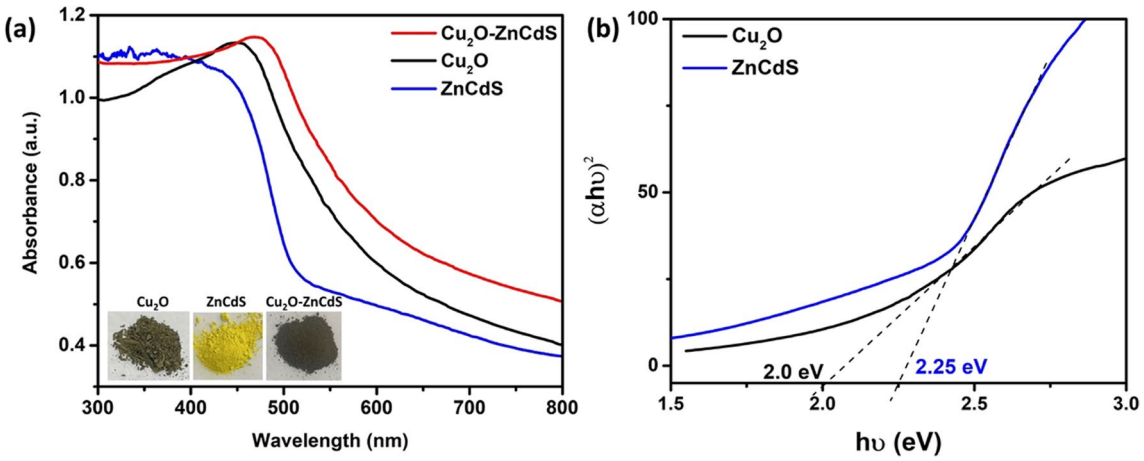

Fig. 4 UV–visible diffuse reflectance spectra (**a**) and corresponding *tauc* plot (**b**) for Cu_2O, ZnCdS and Cu_2O-ZnCdS; the insets (**a**) are the digital photographs of Cu_2O, ZnCdS and Cu_2O-ZnCdS samples

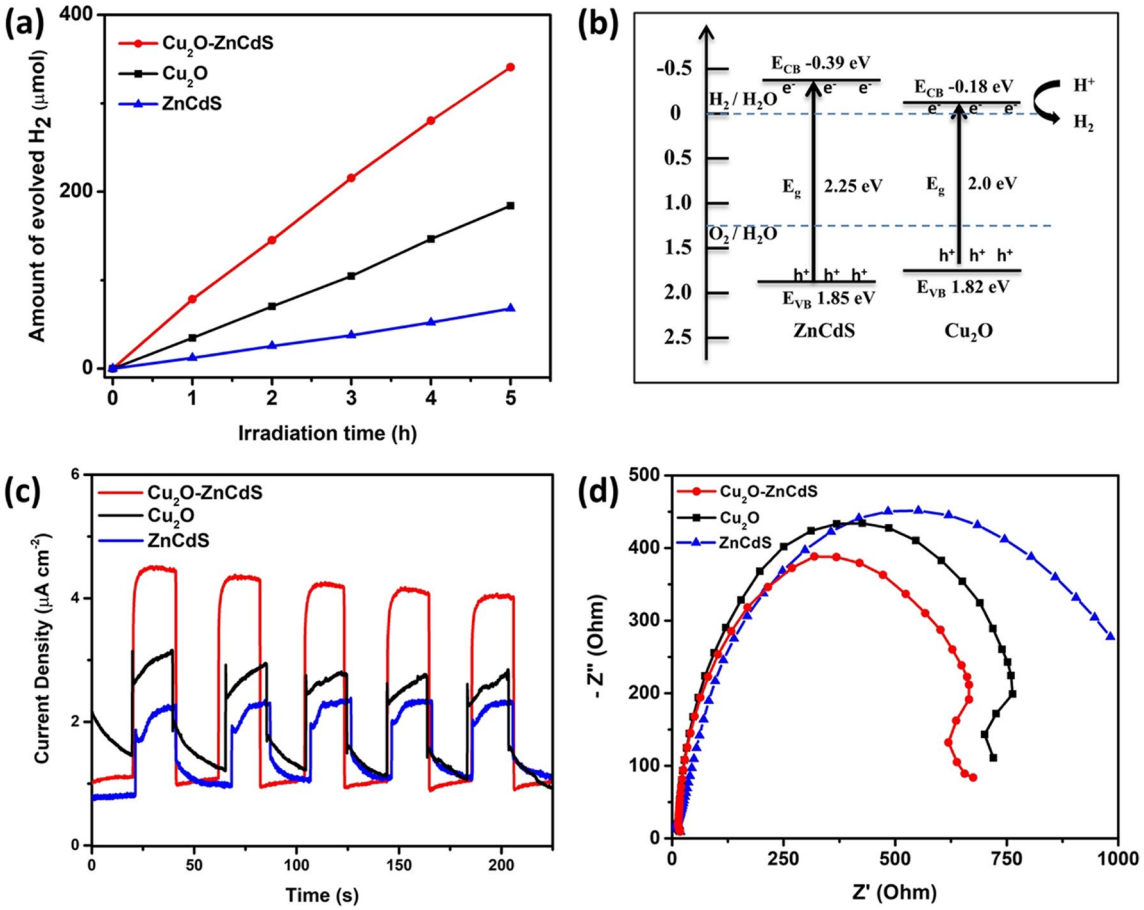

Fig. 5 Time courses of photocatalytic H_2 evolution from water splitting (**a**); A schematic diagram illustrating the band positions and charge transfer process (**b**), Photocurrent response vs. time (**c**) and Nyquist plot curves from EIS (**d**) for Cu_2O, ZnCdS and Cu_2O-ZnCdS composite

a heterojunction is an effective strategy that has been the most widely used in the past few decades. The heterojunction formation is known to overcome the serious drawbacks of fast charge recombination and the limited visible-light absorption of semiconductor photocatalysts [40–42]. Both these factors can refer to the enhanced photocatalytic activity

for Cu_2O-loaded ZnCdS photocatalysts. We have previously observed the effect of loading amount in the composite catalysts (α-Fe_2O_3/$Zn_{0.4}Cd_{0.6}S$) for photocatalytic H_2 production. It was observed that the optimum loading amount to get the highest H_2 evolution rate was 10wt% [29]. The higher loading amount results in the agglomeration of nanoparticles, which reduces the available surface area for photocatalysis. The composite coverage is low at a lower loading amount, resulting in less active sites for interface contact and charge transfer and a lower H_2 production rate.

Moreover, in order to understand the charge transfer process, the band alignments were also calculated for as-synthesized materials. Several theories appear to produce band offset values that are reasonably consistent with the experiment, which include electron affinities, Schottky barrier heights, bulk band structures and effective midgap energies corresponding to charge neutrality. The experimental techniques, including optical spectroscopy, XPS and electrical measurements, are also used for band offset measurement. However, the Kraut approach and Anderson's rule are among the two popular approaches, where Anderson's rule predicts the band alignment based on measurements of separate materials, and the Kraut approach directly measures the band offset [43, 44]. The Kraut's approach gives only a single offset between the bands during single measurements and multiple measurements are required during interface formation for detailed band bending, which requires in-situ experiments. Thus, Anderson's rule has been applied to assess the band alignment, where effective electronegativity of the materials can be used to construct a heterostructure band diagram using electronegativity and band gap values. Despite its conceptual simplicity, the method produces electron energies in reasonably quantitative agreement with the experiment and has been applied to assess the band energies of several semiconductors [45, 46]. However, the method is based solely on chemical composition and cannot account for the effects of bonding, crystal structure and interface interaction, and results may vary with experimental values [47].

The values for conduction (CB) and valence band (VB) potentials were calculated by following equations [48, 49].

$$E_{VB} = X - E_e + 0.5\,E_g \tag{1}$$

$$E_{CB} = E_{VB} - E_g \tag{2}$$

where E_{VB} and E_{CB} are the VB and CB potentials, respectively, E_g is the band-gap energy, E_e is the energy of the free electrons on the hydrogen scale, and X is the absolute electronegativity. The band gap energy values were calculated using *Tauc* plot, and corresponding VB and CB positions were obtained for ZnCdS nanoparticles (E_{VB} = 1.85 eV, E_{CB} = − 0.39 eV) and Cu_2O (E_{VB} = 1.82 eV, E_{CB} = − 0.18 eV). The calculated band edge positions are referred to the standard electrode potential (H^+/H_2 reference energy − 4.44 eV). The band energy diagrams for ZnCdS and Cu_2O are depicted in Fig. 5b, and the results confirm that Cu_2O -ZnCdS can form an overlapping band structure. It can be seen, the VB for ZnCdS is lower compared to Cu_2O, while the CB is higher [50]. Therefore, when the material is irradiated, the electrons are excited from the VB to CB of ZnCdS. Then, the photoinduced electrons in the CB of ZnCdS move to the CB of Cu_2O, generating thus an accumulation of electrons in CB of Cu_2O (where the H_2 reaction occurs) and an accumulation of holes in the VB of Cu_2O (where the sacrificial agent consumes the holes, thus forming a type-I heterojunction [51, 52]. This type I heterojunction system has been known to enhance the charge separation process and improve photocatalytic performance greatly, such as in ZnS/MoS2 and ZnS@Cu3P heterojunction [53–56].

The transient photocurrent responses also show that the photocurrent value of the Cu_2O-ZnCdS electrode is about twice that of bare Cu_2O and ZnCdS, indicating there is less recombination and faster photogenerated electron migration on composite. (Fig. 5c) The enhanced charge separation occurring at Cu_2O-ZnCdS might result from the favorable synergy and band alignment of individual components [57, 58]. The structural and electronic effects might also occur at the junction of Cu_2O-ZnCdS heterojunction, which are responsible for the promotion of charge carrier separation as observed in the case of coexposed anatase (001)–(101) surfaces [59].

The Nyquist plots from EIS also show smaller resistance for Cu_2O-ZnCdS heterojunction, facilitating faster interface charge transfer. (Fig. 5d) The diameter of Cu_2O-ZnCdS is lower than that of Cu_2O and ZnCdS, indicating that the resistance of the charge movement was significantly lower at the interface, which is beneficial to an acceleration of the electrochemical reactions and separation of photoinduced electron–hole pairs [60, 61]. The conductivity enhancement at Cu_2O-ZnCdS is attributed to the interface effect and the local electric field resulting from electron redistribution in the interface area, which enhances the contact field between the electrolyte and electrode and thus boosts the conductivity of the composite [62, 63].

Furthermore, the photocatalytic activity for photodegradation of methylene blue (MB) was also examined under visible light illumination for as-prepared catalysts. Figure 6 shows the MB photocatalytic degradation versus time for solution with Cu_2O, ZnCdS and Cu_2O-ZnCdS catalysts. As can be seen, there is no significant change in dye concentration under dark conditions after 30 min. (Fig. S3) However, a weak photodegradation was observed for Cu_2O under visible light irradiation and ZnCdS samples. (Fig. 6a,b) Such behaviours can be assigned to the large band gap energy and incapable performance under visible light conditions [64,

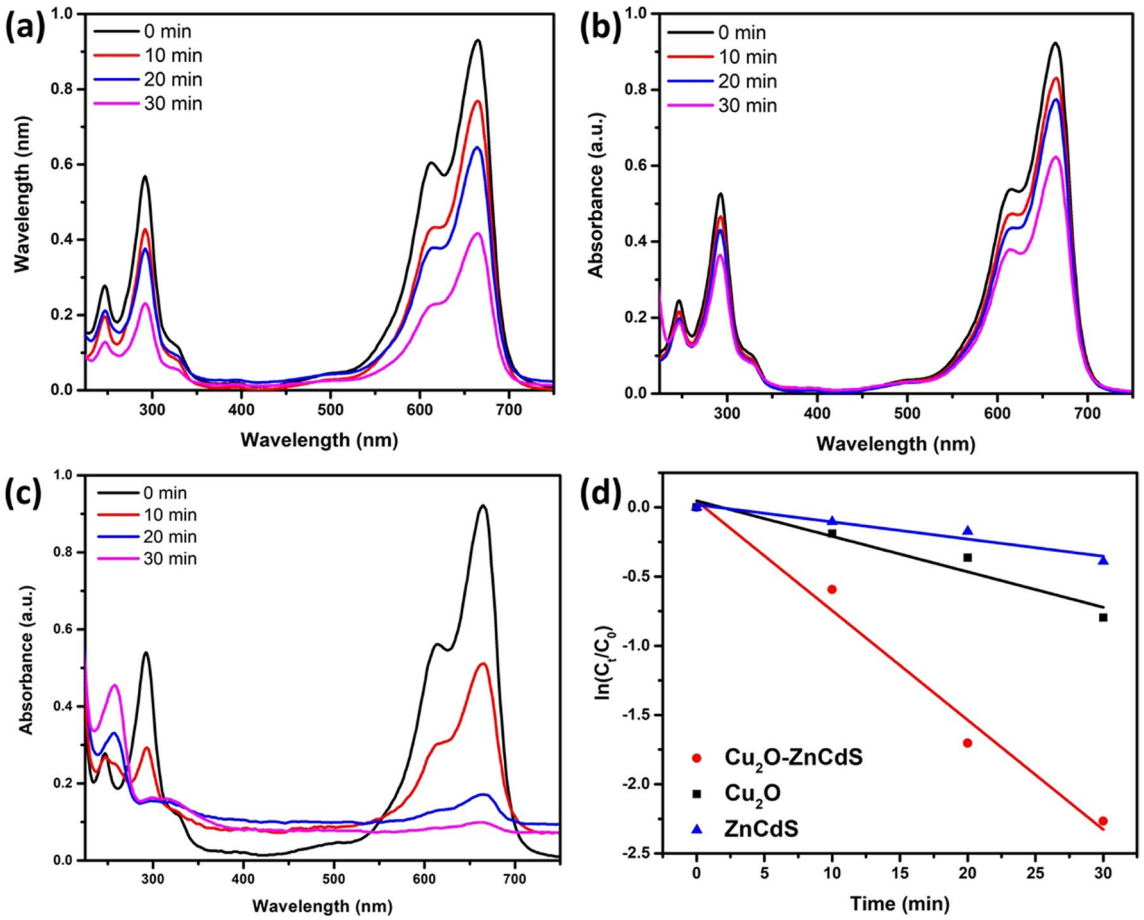

Fig. 6 Change in methylene blue (ME) absorbance in UV–vis spectra over time under visible light irradiation for Cu_2O nanosphere (**a**), ZnCdS nanoparticles (**b**), Cu_2O-ZnCdS composite (**c**), and corresponding reaction kinetics (**d**)

65]. However, in the case of the Cu_2O-ZnCdS catalyst, the degradation process of the pollutant accelerated by increasing the time of irradiation and almost completely degraded after 30 min of irradiation. (Fig. 6c) The photocatalytic kinetics under the visible light illumination for each sample was also investigated with a pseudo-first-order based on the following Eq. 3;

$$ln\left(C_t/C_0\right) = kt \tag{3}$$

In the above equation, the "k" represents the rate constant, "t" is the time of illumination and "C_0 and C_t" are the initial and final concentrations before and after the irradiation, respectively. The k values were calculated using the slope of plots of $ln(C_t/C_0)$ against t, as shown in Fig. 6d. The rate constant for MB degradation over the Cu_2O and ZnCdS samples is 0.025 min^{-1}, 0.012 min^{-1}, respectively. The rate constant for Cu_2O-ZnCdS was calculated to be 0.079 min^{-1}, which is higher compared to individual components. This result strongly indicates that trapping the electrons enhances the photocatalytic reactions, consequently hindering the recombination of electron–hole pairs efficiently, and the whole process is kinetically facilitated [66]. According to the above results, the heterojunction formation by loading ZnCdS into Cu_2O can boost the overall photocatalytic activity for both H_2 production and dye degradation. Hence, these results highlight that the application of composite materials with different semiconductors is significantly important to have synergistic effects and a modified electronic transition to boost the photocatalytic activity compared to the individual components.

4 Conclusion

In conclusion, we have successfully prepared the Cu_2O-ZnCdS composite. TEM, XRD, and XPS analysis confirmed the composite's morphology, crystal structure and elemental composition. Moreover, the optical properties were also measured by UV–vis DRS studies to understand the electronic transition and visible light response. The composite showed a photocatalytic H_2 production rate of

78.50 µmol g^{-1} h^{-1}, which is surprisingly higher than that of individual components. Enhanced performance is mainly attributed to heterojunction formation in composite, which facilitates charge separation as evidenced by transient photocurrent response and EIS data. The Cu_2O-ZnCdS composite also showed photocatalytic degradation performance for dye-ME with a higher rate constant value (0.079 min^{-1}). The improvement in reaction kinetics after heterojunction formation clearly points towards intimate contact between individual components, facilitating the charge carrier in reaction participation and promoting stability. It was observed that coupling the semiconductors improves the photocatalytic performance dramatically, which can help design photo catalytically active catalysts.

Supplementary Information The online version contains supplementary material available at https://doi.org/10.1007/s42247-024-00654-9.

Acknowledgements The authors acknowledge financial support made possible by Qatar University grant # QUCG-CAM-22/23-504. Research reported in this publication was supported by the Qatar Research Development and Innovation Council ARG01-0524-230315. The content is solely the responsibility of the authors and does not necessarily represent the official vies of Qatar Research Development and Innovation Council.

Author contributions Muhammad Imran, Ammar Bin Yousaf, Muhammad Farooq and Peter Kasak contributed to the study conception and design. All authors performed material preparation, formal analysis, data collection and analysis. Supervision was done by Peter Kasak and Muhammad Farooq. Funding acquisition was done by Peter Kasak. Muhammad Imran and Ammar Bin Yousaf wrote the first draft of the manuscript and all authors read and approved the final manuscript.

Funding Open Access funding provided by the Qatar National Library.

Data availability Supporting information as experimental, Figure S1: SEM and TEM image of Cu_2O nanosphere (a, b), ZnCdS nanoparticles (c), and Cu_2O-ZnCdS composite; Figure S2. Survey XPS spectra for Cu_2O-ZnCdS composite; Figure S3.Change in MB absorbance over time under dark conditions for Cu_2O-ZnCdS composite are available free of charge on Emergent Materials webpage at doi:

Declarations

Competing interests The authors declare that they have no competing interests.

References

1. R. Al-Tohamy, S.S. Ali, F. Li, K.M. Okasha, Y.A.G. Mahmoud, T. Elsamahy et al., A critical review on the treatment of dye-containing wastewater: ecotoxicological and health concerns of textile dyes and possible remediation approaches for environmental safety. Ecotoxicol. Environ. Saf. **231**, 113160 (2022). https://doi.org/10.1016/j.ecoenv.2021.113160
2. M. Höök, X. Tang, Depletion of fossil fuels and anthropogenic climate change-a review. Energy Policy **52**, 797–809 (2013). https://doi.org/10.1016/j.enpol.2012.10.046
3. A. Haryanto, S. Fernando, N. Murali, S. Adhikari, Current status of hydrogen production techniques by steam reforming of ethanol: a review. Energy Fuels **19**, 2098–2106 (2005). https://doi.org/10.1021/ef0500538
4. S. Anil, S. Indraja, R. Singh, S. Appari, B. Roy, A review on ethanol steam reforming for hydrogen production over Ni/Al2O3 and Ni/CeO2 based catalyst powders. Int. J. Hydrogen Energy **47**, 8177–8213 (2022). https://doi.org/10.1016/j.ijhydene.2021.12.183
5. J.C. Ehlers, A.A. Feidenhans'l, K.T. Therkildsen, G.O. Larrazábal, Affordable green hydrogen from alkaline water electrolysis: key research needs from an industrial perspective. ACS Energy Lett. **8**, 1502–9 (2023). https://doi.org/10.1021/acsenergylett.2c02897
6. M. Gopinath, R. Marimuthu, A review on solar energy-based indirect water-splitting methods for hydrogen generation. Int. J. Hydrogen Energy **47**, 37742–37759 (2022). https://doi.org/10.1016/j.ijhydene.2022.08.297
7. M. Mehrpooya, R. Habibi, A review on hydrogen production thermochemical water-splitting cycles. J. Clean. Prod. **275**, 123836 (2020). https://doi.org/10.1016/j.jclepro.2020.123836
8. V.A. Panchenko, Y.V. Daus, A.A. Kovalev, I.V. Yudaev, Y.V. Litti, Prospects for the production of green hydrogen: review of countries with high potential. Int. J. Hydrogen Energy **48**, 4551–4571 (2023). https://doi.org/10.1016/j.ijhydene.2022.10.084
9. H. Ishaq, I. Dincer, C. Crawford, A review on hydrogen production and utilization: challenges and opportunities. Int. J. Hydrogen Energy **47**, 26238–26264 (2022). https://doi.org/10.1016/j.ijhydene.2021.11.149
10. J. Corredor, M.J. Rivero, C.M. Rangel, F. Gloaguen, I. Ortiz, Comprehensive review and future perspectives on the photocatalytic hydrogen production. J. Chem. Technol. Biotechnol. **94**, 3049–3063 (2019). https://doi.org/10.1002/jctb.6123
11. S. Dutta, B. Gupta, S.K. Srivastava, A.K. Gupta, Recent advances on the removal of dyes from wastewater using various adsorbents: a critical review. Mater Adv **2**, 4497–4531 (2021). https://doi.org/10.1039/d1ma00354b
12. M. Shabir, M. Yasin, M. Hussain, I. Shafiq, P. Akhter, A.S. Nizami et al., A review on recent advances in the treatment of dye-polluted wastewater. J. Ind. Eng. Chem. **112**, 1–19 (2022). https://doi.org/10.1016/j.jiec.2022.05.013
13. K. Sathya, K. Nagarajan, G. Carlin Geor Malar, S. Rajalakshmi, P. Raja Lakshmi, A comprehensive review on comparison among effluent treatment methods and modern methods of treatment of industrial wastewater effluent from different sources. Appl Water Sci **12**, 1–27 (2022). https://doi.org/10.1007/s13201-022-01594-7
14. M. Ahmed, M.O. Mavukkandy, A. Giwa, M. Elektorowicz, E. Katsou, O. Khelifi et al., Recent developments in hazardous pollutants removal from wastewater and water reuse within a circular economy. npj Clean Water **5**, 1–25 (2022). https://doi.org/10.1038/s41545-022-00154-5
15. S. Velusamy, A. Roy, S. Sundaram, M.T. Kumar, A review on heavy metal ions and containing dyes removal through graphene oxide-based adsorption strategies for textile wastewater treatment. Chem. Rec. **21**, 1570–1610 (2021). https://doi.org/10.1002/tcr.202000153

16. H. Zangeneh, A.A.L. Zinatizadeh, M. Habibi, M. Akia, I.M. Hasnain, Photocatalytic oxidation of organic dyes and pollutants in wastewater using different modified titanium dioxides: a comparative review. J. Ind. Eng. Chem. **26**, 1–36 (2015). https://doi.org/10.1016/j.jiec.2014.10.043
17. S.D. Tilley, Will cuprous oxide really make it in water-splitting applications? ACS Energy Lett. **8**, 2338–2344 (2023). https://doi.org/10.1021/acsenergylett.3c00578
18 C.-f Li, R.-t Guo, Z.-r Zhang, T. Wu, W.-g Pan, Converting CO2 into value-added products by Cu2O-based catalysts: from photocatalysis, electrocatalysis to photoelectrocatalysis. Small **2207875**, 1–31 (2023). https://doi.org/10.1002/smll.202207875
19. B.A. Koiki, O.A. Arotiba, Cu2O as an emerging semiconductor in photocatalytic and photoelectrocatalytic treatment of water contaminated with organic substances: a review. RSC Adv. **10**, 36514–36525 (2020). https://doi.org/10.1039/d0ra06858f
20. K. Wang, X. Yu, F. Yang, Z. Liu, Z. Li, T. Zhang et al., Research progress on Cu2O-based type-II heterojunction photocatalysts for photocatalytic removal of antibiotics. ChemistrySelect **7**, e202202186 (2022). https://doi.org/10.1002/slct.202202186
21. T.N.Q. Trang, L.T.N. Tu, T.V. Man, M. Mathesh, N.D. Nam, V.T.H. Thu, A high-efficiency photoelectrochemistry of Cu2O/TiO2 nanotubes based composite for hydrogen evolution under sunlight. Compos. Part B Eng. **174**, 106969 (2019). https://doi.org/10.1016/j.compositesb.2019.106969
22. A. Piątkowska, D. Moszyński, S. Mozia, Enhanced solar light photocatalytic activity of TiO_2 modified with ammonium carbamate for the removal of ketoprofen from water. J Water Process Eng **56**, 104534 (2023). https://doi.org/10.1016/j.jwpe.2023.104534
23. A. Piątkowska, K. Szymański, S. Mozia, Effect of sulfur on the solar light photoactivity of TiO_2-based photocatalysts. Chem. Eng. Res. Des. **195**, 721–731 (2023). https://doi.org/10.1016/j.cherd.2023.04.049
24. Q. Su, C. Zuo, M. Liu, X. Tai, A review on Cu2O-based composites in photocatalysis: synthesis, modification, and applications. Molecules **28**, 5576 (2023)
25. A.M. Mohammed, S.S. Mohtar, F. Aziz, S.A. Mhamad, M. Aziz, Review of various strategies to boost the photocatalytic activity of the cuprous oxide-based photocatalyst. J. Environ. Chem. Eng. **9**, 105138 (2021). https://doi.org/10.1016/j.jece.2021.105138
26 Y.H. Zhang, M.M. Liu, J.L. Chen, S.M. Fang, P.P. Zhou, Recent advances in Cu2O-based composites for photocatalysis: a review. Dalt. Trans. **50**, 4091–111 (2021). https://doi.org/10.1039/d0dt04434b
27. H. Bao, W. Zhang, Q. Hua, Z. Jiang, J. Yang, W. Huang, Crystal-plane-controlled surface restructuring and catalytic performance of oxide nanocrystals. Angew. Chem. - Int Ed **50**, 12294–12298 (2011). https://doi.org/10.1002/anie.201103698
28. C. Zheng, J. Cao, Y. Zhang, H. Zhao, Insight into the oxidation mechanism of a cu-based oxygen carrier (cu → Cu2O → CuO) in chemical looping combustion. Energy Fuels **34**, 8718–8725 (2020). https://doi.org/10.1021/acs.energyfuels.0c00941
29 M. Imran, Yousaf A. Bin, P. Kasak, A. Zeb, S.J. Zaidi, Highly efficient sustainable photocatalytic Z-scheme hydrogen production from an A-Fe2O3 engineered ZnCdS heterostructure. J. Catal. **353**, 81–8 (2017). https://doi.org/10.1016/j.jcat.2017.06.019
30. Z. He, Y. Xia, B. Tang, X. Jiang, J. Su, Fabrication and photocatalytic property of ZnO/Cu2O core-shell nanocomposites. Mater. Lett. **184**, 148–151 (2016). https://doi.org/10.1016/j.matlet.2016.08.020
31. D. Zhao, C.M. Tu, X.J. Hu, N. Zhang, Notable in situ surface transformation of Cu2O nanomaterials leads to dramatic activity enhancement for CO oxidation. RSC Adv. **7**, 37596–37603 (2017). https://doi.org/10.1039/c7ra05950g
32. J. Mohapatra, Defect-related blue emission from ultra-fine Zn1−xCdxS quantum dots synthesized by simple beaker chemistry. Int. Nano Lett. **3**, 1–8 (2013). https://doi.org/10.1186/2228-5326-3-31
33. H. Qin, Z. Wang, S. Yang, W. Jiang, Y. Gu, J. Chen et al., High efficiency degradation of 2,4-dichlorophenol using Cu2S/Cu2O decorated nanoscale zerovalent iron via adsorption and photocatalytic performances. J. Clean. Prod. **378**, 134587 (2022). https://doi.org/10.1016/j.jclepro.2022.134587
34. H. Wang, M. Soldemo, D. Degerman, P. Lömker, C. Schlueter, A. Nilsson et al., Direct evidence of subsurface oxygen formation in oxide-derived Cu by X-ray photoelectron spectroscopy. Angew. Chem. **134**, e202111021 (2022). https://doi.org/10.1002/ange.202111021
35. T. Ghodselahi, M.A. Vesaghi, A. Shafiekhani, A. Baghizadeh, M. Lameii, XPS study of the Cu@Cu 2 O core-shell nanoparticles. Appl. Surf. Sci. **255**, 2730–2734 (2008). https://doi.org/10.1016/j.apsusc.2008.08.110
36. C. Wang, H. Tissot, C. Escudero, V. Pérez-Dieste, D. Stacchiola, J. Weissenrieder, Redox properties of Cu2O(100) and (111) surfaces. J. Phys. Chem. C **122**, 28684–28691 (2018). https://doi.org/10.1021/acs.jpcc.8b08494
37. V. Hayez, A. Franquet, A. Hubin, H. Terryn, XPS study of the atmospheric corrosion of copper alloys of archaeological interest. Surf. Interface Anal. **36**, 876–879 (2004). https://doi.org/10.1002/sia.1790
38. X. Hao, D. Xiang, Z. Jin, Zn-vacancy engineered S-scheme ZnCdS/ZnS photocatalyst for highly efficient photocatalytic H2 evolution. ChemCatChem **13**, 4738–4750 (2021). https://doi.org/10.1002/cctc.202100994
39. B. Ben Salem, G. Essalah, S. Ben Ameur, B. Duponchel, H. Guermazi, S. Guermazi et al., Synthesis and comparative study of the structural and optical properties of binary ZnO-based composites for environmental applications. RSC Adv. **13**, 6287–6303 (2023). https://doi.org/10.1039/d2ra07837f
40. H. Wang, L. Zhang, Z. Chen, J. Hu, S. Li, Z. Wang et al., Semiconductor heterojunction photocatalysts: design, construction, and photocatalytic performances. Chem. Soc. Rev. **43**, 5234–5244 (2014). https://doi.org/10.1039/c4cs00126e
41. J. Low, J. Yu, M. Jaroniec, S. Wageh, A.A. Al-Ghamdi, Heterojunction photocatalysts. Adv. Mater. **29**, 1601694 (2017). https://doi.org/10.1002/adma.201601694
42. G. Di Liberto, L.A. Cipriano, S. Tosoni, G. Pacchioni, Rational Design of Semiconductor Heterojunctions for photocatalysis. Chem - A Eur J **27**, 13306–13317 (2021). https://doi.org/10.1002/chem.202101764
43. E.T. Yu, J.O. McCaldin, T.C. McGill, Band offsets in semiconductor heterojunctions. **46**, (1992). https://doi.org/10.1016/S0081-1947(08)60397-5
44. L.G. Di, G. Pacchioni, Band offset in semiconductor heterojunctions. J. Phys. Condens. Matter **33**, 415002 (2021). https://doi.org/10.1088/1361-648X/ac1620
45. Y. Xu, M.A.A. Schoonen, The absolute energy positions of conduction and valence bands of selected semiconducting minerals. Am. Mineral. **85**, 543–556 (2000). https://doi.org/10.2138/am-2000-0416
46. I.E. Castelli, T. Olsen, S. Datta, D.D. Landis, S. Dahl, K.S. Thygesen et al., Computational screening of perovskite metal oxides for optimal solar light capture. Energy Environ. Sci. **5**, 5814–5819 (2012). https://doi.org/10.1039/c1ee02717d
47. G. Di Liberto, S. Tosoni, G. Pacchioni, Nature and role of surface junctions in $BiOIO_3$ photocatalysts. Adv. Funct. Mater. **31**, 2009472 (2021). https://doi.org/10.1002/adfm.202009472
48. M.A. Butler, D.S. Ginley, Prediction of flatband potentials at semiconductor-electrolyte interfaces from atomic electronegativities. J. Electrochem. Soc. **125**, 228–232 (1978). https://doi.org/10.1149/1.2131419

49. Y Il. Kim, S.J. Atherton, E.S. Brigham, T.E. Mallouk, Sensitized layered metal oxide semiconductor particles for photochemical hydrogen evolution from nonsacrificial electron donors. J. Phys. Chem. **97**, 11802–10 (1993). https://doi.org/10.1021/j100147a038
50. Q. Li, H. Meng, P. Zhou, Y. Zheng, J. Wang, J. Yu et al., Zn1-xCdxS solid solutions with controlled bandgap and enhanced visible-light photocatalytic H2-production activity. ACS Catal. **3**, 882–889 (2013). https://doi.org/10.1021/cs4000975
51. X. Qiao, C. Pan, Y. Dong, G. Wang, H. Zhang, Y. Leng et al., P-type Cu2O as an effective interlayer between CdS and NiO: xcocatalysts to promote photocatalytic hydrogen production. New J. Chem. **44**, 17719–17723 (2020). https://doi.org/10.1039/d0nj04206d
52. M. Nolan, S.D. Elliott, The p-type conduction mechanism in Cu2O: a first principles study. Phys. Chem. Chem. Phys. **8**, 5350–5358 (2006). https://doi.org/10.1039/b611969g
53. W. Cai, F. Zhang, Y. Wang, D. Li, A novel I-type 0D/0D ZnS@Cu3P heterojunction for photocatalytic hydrogen evolution. Inorg. Chem. Commun. **134**, 109046 (2021). https://doi.org/10.1016/j.inoche.2021.109046
54. J.E. Samaniego-Benitez, L. Lartundo-Rojas, A. García-García, H.A. Calderón, A. Mantilla, One-step synthesis and photocatalytic behavior for H2 production from water of ZnS/MoS2 composite material. Catal. Today **360**, 99–105 (2021). https://doi.org/10.1016/j.cattod.2019.08.011
55. S.J.A. Moniz, S.A. Shevlin, D.J. Martin, Z.X. Guo, J. Tang, Visible-light driven heterojunction photocatalysts for water splitting-a critical review. Energy Environ. Sci. **8**, 731–759 (2015). https://doi.org/10.1039/c4ee03271c
56. P. Xia, X. Feng, R.J. Ng, S. Wang, D. Chi, C. Li et al., Impact and origin of interface states in MOS capacitor with monolayer MoS 2 and HfO 2 high-k dielectric. Sci. Rep. **7**, 1–9 (2017). https://doi.org/10.1038/srep40669
57. G. Di Liberto, S. Tosoni, G. Pacchioni, Role of heterojunction in charge carrier separation in coexposed anatase (001)-(101) surfaces. J. Phys. Chem. Lett. **10**, 2372–2377 (2019). https://doi.org/10.1021/acs.jpclett.9b00504
58. L. Lo Presti, V. Pifferi, G. Di Liberto, G. Cappelletti, L. Falciola, G. Cerrato et al., Direct measurement and modeling of spontaneous charge migration across anatase-brookite nanoheterojunctions. J. Mater. Chem. A **9**, 7782–7790 (2021). https://doi.org/10.1039/d1ta01040a
59. G. Di Liberto, V. Pifferi, L. Lo Presti, M. Ceotto, L. Falciola, Atomistic explanation for interlayer charge transfer in metal-semiconductor nanocomposites: the case of silver and anatase. J. Phys. Chem. Lett. **8**, 5372–5377 (2017). https://doi.org/10.1021/acs.jpclett.7b02555
60. J. Garcia-Barriocanal, A. Rivera-Calzada, M. Varela, Z. Sefrioui, E. Iborra, C. Leon et al., Colossal ionic conductivity at interfaces of epitaxial ZrO2:Y2O3/SrTiO3 heterostructures. Science (80-) **321**, 676–80 (2008)
61. B. Zhu, P.D. Lund, R. Raza, Y. Ma, L. Fan, M. Afzal et al., Schottky junction effect on high performance fuel cells based on nanocomposite materials. Adv. Energy Mater. **5**, 1–6 (2015). https://doi.org/10.1002/aenm.201401895
62. X. Cheng, S. Gu, A. Centeno, G. Dawson, Plasmonic enhanced Cu 2 O-Au-BFO photocathodes for solar hydrogen production. Sci. Rep. **9**, 1–8 (2019). https://doi.org/10.1038/s41598-019-41613-3
63. M. Alhaddad, R.M. Navarro, M.A. Hussein, R.M. Mohamed, Visible light production of hydrogen from glycerol over Cu2O-gC3N4 nanocomposites with enhanced photocatalytic efficiency. J. Mater. Res. Technol **9**, 15335–15345 (2020). https://doi.org/10.1016/j.jmrt.2020.10.093
64. Z. Ye, L. Kong, F. Chen, Z. Chen, Y. Lin, C. Liu, A comparative study of photocatalytic activity of ZnS photocatalyst for degradation of various dyes. Optik (Stuttg) **164**, 345–354 (2018). https://doi.org/10.1016/j.ijleo.2018.03.030
65. X. Lu, J. Huang, H. Xie, W. Huang, Z. Sun, D. Zhang, The enhanced photocatalytic performance of pr doped Cu2O under visible light. ChemistrySelect **8**, e202204756 (2023). https://doi.org/10.1002/slct.202204756
66. X. Zhang, M. Xia, F. Wang, W. Lei, Cu2O/MoS2 composites: a novel photocatalyst for photocatalytic degradation of organic dyes under visible light. Ionics (Kiel) **26**, 6359–6369 (2020). https://doi.org/10.1007/s11581-020-03749-5